

Facile fabrication of highly flexible, porous PEDOT:PSS/SWCNTs films for thermoelectric applications

Fu-Wei Liu(刘福伟), Fei Zhong(钟飞), Shi-Chao Wang(王世超), Wen-He Xie(谢文合), Xue Chen(陈雪),Ya-Ge Hu(胡亚歌), Yu-Ying Ge(葛钰莹), Yuan Gao(郜源), Lei Wang(王雷), and Zi-Qi Liang(梁子骐)
Citation: Chin. Phys. B, 2022, 31 (**2**): 027303. DOI: 10.1088/1674-1056/ac3502
Journal homepage: http://cpb.iphy.ac.cn; http://iopscience.iop.org/cpb

What follows is a list of articles you may be interested in

Enhanced thermoelectric properties in two-dimensional monolayer Si_2BN by adsorbing halogen atoms

Cheng-Wei Wu(吴成伟), Changqing Xiang(向长青), Hengyu Yang(杨恒玉), Wu-Xing Zhou(周五星), Guofeng Xie(谢国锋), Baoli Ou(欧宝立), and Dan Wu(伍丹)
Chin. Phys. B, 2021, 30 (**3**): 037304. DOI: 10.1088/1674-1056/abd163

Electronic and thermoelectric properties of alkali metal-based perovskites $CsYbF_3$ and $RbYbF_3$

Q Mahmood, N A Noor, T Ghrib, Nessrin A Kattan, Asif Mahmood, and Shahid M Ramay
Chin. Phys. B, 2020, 29 (**11**): 117305. DOI: 10.1088/1674-1056/ab9de3

Influence of spherical inclusions on effective thermoelectric properties of thermoelectric composite materials

Wen-Kai Yan(闫文凯), Ai-Bing Zhang(张爱兵), Li-Jun Yi(易利军), Bao-Lin Wang(王保林), Ji Wang(王骥)
Chin. Phys. B, 2020, 29 (**5**): 057301. DOI: 10.1088/1674-1056/ab7d96

Strategies for optimizing the thermoelectricity of PbTe alloys

Jinze Zhai(翟近泽), Teng Wang(王腾), Hongchao Wang(王洪超), Wenbin Su(苏文斌), Xue Wang(王雪), Tingting Chen(陈婷婷), Chunlei Wang(王春雷)
Chin. Phys. B, 2018, 27 (**4**): 047306. DOI: 10.1088/1674-1056/27/4/047306

Impact of coupling geometry on thermoelectric properties of oligophenyl-base transistor

S Ramezani Akbarabadi, H Rahimpour Soleimani, M Bagheri Tagani, Z Golsanamlou
Chin. Phys. B, 2017, 26 (**2**): 027303. DOI: 10.1088/1674-1056/26/2/027303

SPECIAL TOPIC — Organic and hybrid thermoelectrics

Facile fabrication of highly flexible, porous PEDOT:PSS/SWCNTs films for thermoelectric applications

Fu-Wei Liu(刘福伟)[1,†], Fei Zhong(钟飞)[2,†], Shi-Chao Wang(王世超)[2], Wen-He Xie(谢文合)[1], Xue Chen(陈雪)[1], Ya-Ge Hu(胡亚歌)[1], Yu-Ying Ge(葛钰莹)[1], Yuan Gao(郜源)[1], Lei Wang(王雷)[2,‡], and Zi-Qi Liang(梁子骐)[3,§]

[1] *College of Physics and Electronic Engineering, Xinyang Normal University, Xinyang* 464000, *China*

[2] *Shenzhen Key Laboratory of Polymer Science and Technology, College of Materials Science and Engineering, Shenzhen University, Shenzhen* 518060, *China*

[3] *Department of Materials Science, Fudan University, Shanghai* 200433, *China*

(Received 31 August 2021; revised manuscript received 14 October 2021; accepted manuscript online 1 November 2021)

High-performance organic composite thermoelectric (TE) materials are considered as a promising alternative for harvesting heat energy. Herein, composite films of poly (3,4-ethyienedioxythiophene):poly(styrene sulfonate)/single-walled carbon nanotubes (PEDOT:PSS/SWCNTs) were fabricated by utilizing a convenient solution mixing method. Thereafter, the as-prepared hybrid films were treated using sulfuric acid (H_2SO_4) to further optimize the TE performance. Film morphological studies revealed that the sulfuric acid treated PEDOT:PSS/SWCNTs composite samples all possessed porous structures. Due to the successful fabrication of highly conductive networks, the porous nano-architecture also exhibited much more excellent TE properties when compared with the dense structure of the pristine samples. For the post-treated sample, a high power factor of 156.43 $\mu W{\cdot}m^{-1}{\cdot}K^{-2}$ can be achieved by adjusting the content of CNTs, which is approximately 3 orders of magnitude higher than that of the corresponding untreated samples (0.23 $\mu W{\cdot}m^{-1}{\cdot}K^{-2}$). Besides, the obtained films also showed excellent mechanical flexibility, owing to the porous nanostructure and the strong π–π interactions between the two components. This work indicates that the H_2SO_4 treatment could be a promising strategy for fabricating highly-flexible and porous PEDOT:PSS/SWCNTs films with high TE performances.

Keywords: porous film, thermoelectric properties, flexibility

PACS: 73.50.Lw, 88.30.rh, 78.67.Rb **DOI:** 10.1088/1674-1056/ac3502

1. Introduction

Recently, the demand for eco-efficient, renewable, and sustainable energy, which has attracted a lot of interest, triggers the development of various energy conversion systems.[1–5] Among the most common technologies, flexible thermoelectric (TE) generator can directly convert heat into electrical energy without additional pollution, and is considered an ideal approach to harvest energy for portable and wearable electric devices.[6–9] Considerable attention has been paid to organic TE materials, especially the conductive polymers (CPs) and their nanocomposites for developing high-performance flexible TE generators, through which the large amount of ubiquitous low-quality heat can be effectively utilized as green energy resources.[6,10,11] The energy conversion efficiency of TE materials is generally determined via the dimensionless figure of merit $ZT = S^2\sigma T/\kappa$, where σ, S, T, and κ stand for the electrical conductivity, Seebeck coefficient, absolute temperature, and thermal conductivity, respectively. Obviously, ZT can be improved via either increasing the power factor ($PF = S^2\sigma$) or decreasing the thermal conductivity κ.

Most CPs and their nanocomposites exhibit relatively low thermal conductivity, in general less than 1 $W{\cdot}m^{-1}{\cdot}K^{-1}$ (around 1–3 orders of magnitude lower than that of the inorganic TE materials), and they therefore show enormous potential in TE applications if an ideal σ and S can be obtained.[7,12] Thus far, continuous attempts have been made to improve the power factor of the typical CPs, such as polyaniline (PANI), polypyrrole (PPy), polycarbazole (PCarb), polythiophene (PTH), and their derivatives. Specifically, poly(3,4-ethylenedioxythiophene):polystyrene-sulfonate (PEDOT:PSS) as a typical derivative of PTH, possesses unique solution processability, excellent environmental stability, and relatively high electrical conductivity, offering the possibility of realizing even higher power factor, and is considered one of the most ideal organic TE materials.[6,9] Besides, the PEDOT:PSS film also shows excellent flexibility, light weight, and commercial availability, which provides an opportunity for large-scale application in portable TE devices.

To further increase the power factor, it has been proposed to separate PSS from PEDOT:PSS for achieving crystalline PEDOT with additive such as surfactants,[13,14] organic solvents,[15,16] ionic liquids,[17,18] and inorganic salts,[19,20] as well as post-treatment by immersing PEDOT:PSS films

[†]These authors contributed equally.

[‡]Corresponding author. E-mail: wl@szu.edu.cn

[§]Corresponding author. E-mail: zqliang@fudan.edu.cn

© 2022 Chinese Physical Society and IOP Publishing Ltd

into polar solvents (e.g., DMSO,[21,22] EG,[23,24] etc.) or acids.[25,26] Besides, introducing inorganic fillers into the PEDOT:PSS matrix has also been demonstrated as an effective method to improve their TE properties. Among various inorganic fillers, carbon nanotubes (CNTs) have attracted a great deal of attention, due to their high conductivity, unique mechanical properties, lightweight, and stability.[26–29] For preparing the CNTs/PEDOT:PSS composites, various methods were conducted, for instance, Yu *et al.* mixed two different CNTs with PEDOT:PSS directly for forming electrically connected junctions, and achieved a maximum ZT of ~ 0.02;[30] Song *et al.* prepared layered nanostructure of PEDOT:PSS/SWCNTs by using a two-step spin casing process, and obtained a maximum power factor of 21.1 $\mu W \cdot m^{-1} \cdot K^{-2}$;[31] Zhang *et al.* fabricated nanocomposites of PEDOT:PSS-coated multi-wall CNTs via an *in situ* polymerization process, which possessed much higher power factor than that of the pure PEDOT:PSS.[32] For further improving the TE properties of the CNTs/PEDOT:PSS composites, solution mixing and post-treatment process were combined. For example, Jiang *et al.* introduced DMSO solution into PEDOT:PSS and then prepared single-walled CNT (SWCNTs)/PEDOT:PSS composite by using a vacuum filtration method, which showed a notable ZT of 0.12;[33] Zhang *et al.* prepared PEDOT:PSS/SWCNTs composite by direct mixing method, and the obtained samples were then dipped into DMSO solution, reaching an optimized power factor of 300 $\mu W \cdot m^{-1} \cdot K^{-2}$.[34] Lee *et al.* investigated the effect of post-treatment using ethylene glycol (EG) on the TE property of CNTs/PEDOT:PSS composite, and the results revealed that after EG treatment, the highest power factor of 151 $\mu W \cdot m^{-1} \cdot K^{-2}$ can be obtained.[35] Du *et al.* fabricated flexible CNTs/PEDOT:PSS composite films and enhanced their power factor to 108.7 $\mu W \cdot m^{-1} \cdot K^{-2}$ via a post-treatment procedure using DMSO.[36]

The above-mentioned results are encouraging and provide potential directions for further research. However, up to now, there are few reports about the design of their morphologies (e.g., porous nanostructures), which is an important factor affecting the thermal conductivity and thus TE properties of the composites.[37] Recently, aiming to suppress the thermal conductivity, aerogel porous structures have been successfully created in PEDOT:PSS-based composites.[38,39] Nevertheless, a large amount of micrometer-sized pores may inevitably reduce the electrical conductivity and the physical mechanical properties. Therefore, it is still a great challenge to develop a porous structure with relatively high electrical conductivity and Seebeck coefficient.

Herein, SWCNTs were incorporated into the PEDOT:PSS solution to fabricate flexible PEDOT:PSS/SWCNTs composite films by using a drop-casting method. Additionally, a post-treatment procedure using sulfuric acid was conducted. It is found that the sulfuric acid treatment can not only improve the crystallinity of PEDOT:PSS, but also change the surface topography of the film.[40] Considering that the hollow CNTs were partially embedded in the PEDOT:PSS matrix, we speculate that the variation of morphology may be extended to the internal part of the whole PEDOT:PSS/SWCNTs composite film after the post-treatment using H_2SO_4. Not surprisingly, the treated samples containing different contents of CNTs all show porous structures. Due to the successful fabrication of highly conductive networks, the treated samples with porous structure also show much more excellent TE properties when compared with the pristine samples with dense structure. After treatment, the samples containing 10 wt% SWCNTs can reach a maximum power factor of 156.43 $\mu W \cdot m^{-1} \cdot K^{-2}$ at room temperature. This work indicates that the H_2SO_4 treatment could be a promising strategy for fabricating highly-flexible and porous PEDOT:PSS/SWCNTs films with high TE performances.

2. Experimental details

2.1. Chemicals

PEDOT:PSS (Clevios PH1000) was received from Heraeus Company (Germany). Sulfuric acid (H_2SO_4, 98%) and nitric acid (HNO_3, 69%) were purchased from Sun Chemical Technology Co., Ltd. (Shanghai, China). All reagents were used as obtained without further purification. SWCNTs with a diameter of less than 3 nm (purity $>$ 95.0 wt%) were obtained from XFNANO Materials Technology Co., Ltd. (Nanjing, China). Deionized water (DW) and ethanol were used throughout the preparation procedure. In the film preparation, 1.00 cm $\times$ 1.00 cm $\times$ 0.05 cm glass sheets were used as substrates.

2.2. Preparation of porous PEDOT:PSS/SWCNTs composite films

To improve the dispersion of CNTs in water, an acid treatment was conducted: a proper amount of CNTs was added to the mixture solution of H_2SO_4/HNO_3 (volume ratio 3/1). The as-prepared mixture was ultrasonically treated for 6 hours at 50 °C, and then the suspension was continuously cleaned by vacuum filtration until the filtrate was neutral. To prepare PEDOT:PSS/SWCNTs composite films, different weight fractions of CNTs (0, 2, 5, 7, 10, 12.5, 15, 20 wt%) were added to the PEDOT:PSS aqueous solution (1 mg/mL), and followed by 1 hour ultrasonic treatment. Afterwards, the mixed solution was cast on glass substrates and dried at room temperature. For the sake of brevity, these as-prepared films were abbreviated as PP, PP-2, PP-5, PP-7, PP-10, PP-12.5, PP-15, and PP-20, respectively. For post-treatment, the as-prepared film samples were H_2SO_4 treated for 24 hours in a warm-water bath

(around 50 °C). And then, the treated samples were washed by using a large amount of DW and ethanol, and followed by a drying process. Finally, the porous PEDOT:PSS/SWCNTs composite films were successfully fabricated. For ease of comparison, the H_2SO_4 treated samples were abbreviated as PP-H, PP-2-H, PP-5-H, PP-7-H, PP-10-H, PP-12.5-H, PP-15-H, and PP-20-H, respectively.

2.3. Characterization and measurements

The morphologies of the samples were examined by a Hitachi S-4700 field emission scanning electron microscope (FE-SEM). The molecular structure changes were investigated by using a Thermo Fisher Nicolet 6700 Fourier transform infrared spectroscopy (FTIR) in the scanning range from 550 cm^{-1} to 4000 cm^{-1}. Raman spectra were collected within a wavenumber range of 500–2000 cm^{-1} using a Renishaw inVia-Feflex confocal Raman microscope (UK) with an excitation wavelength of 514.5 nm. Ultraviolet-visible (UV-Vis) absorption spectra were recorded by using a Thermo Fisher Evolution 220 spectrophotometer (USA) within a wavelength range of 190–1100 nm. X-ray diffraction (XRD) analyses were performed on an x-ray powder diffractometer (Smartlab 9) in the scanning range $2\theta = 5°$–$60°$. The electron binding energies of the polymers were measured using a Thermo Fisher ESCALAB 250Xi x-ray photoelectron spectroscopy (XPS). The Seebeck coefficients and electric conductivities were measured by using a MRS-3 M thin film thermoelectric test system (Wuhan Joule Yacht Science & Technology Co., Ltd, China) under vacuum environment. The carrier mobility and carrier concentration were investigated using a CVM 200 Hall system (Beijing Chenjing Tech Co., Ltd., China).

3. Results and discussion

In this work, we designed and fabricated porous PEDOT:PSS/SWCNTs composite films with high flexibility and excellent thermoelectric properties, by adding SWCNTs to PEDOT:PSS solution and a following post-treatment using H_2SO_4. As shown in Fig. 1, a proper amount of acid treated SWCNTs and PEDOT:PSS were mixed directly to form a dark blue solution, which can be used to prepare PEDOT:PSS/SWCNTs composite films through a facile drop casting strategy. To further improve the TE properties of the as-prepared composite samples, the nonconductive PSS is partly removed via a H_2SO_4 post-treatment. Meanwhile, more ordered conductive structure forms due to the rearrangement of the polymer molecular, and subsequently results in the variation of surface morphology of PEDOT:PSS. Considering that the CNTs possess hollow nanostructure, the incorporation of SWCNTs may promote the diffusion of acid liquid into the composites and thus extend the morphology evolution from surface to the internal part of the whole SWCNTs/PEDOT:PSS film via H_2SO_4 treatment.

To obtain an insight into how the sulfuric acid solution processing affects the nanostructure of PEDOT:PSS and the composites thin films, SEM imaging was applied to characterize the variation of the film morphologies before and after the post-treatment. As shown in Fig. 2, relatively flat surface topography was clearly observed in the pristine PEDOT:PSS sample. With introduction of SWCNTs, the surface of the composite films become much rougher compared to that of the pure PEDOT:PSS film. When the amount of SWCNTs is relatively small, for example, 2 wt% and 5 wt%, long strips of CNTs can only be observed in some section of the film with relatively large space between the adjacent CNTs.

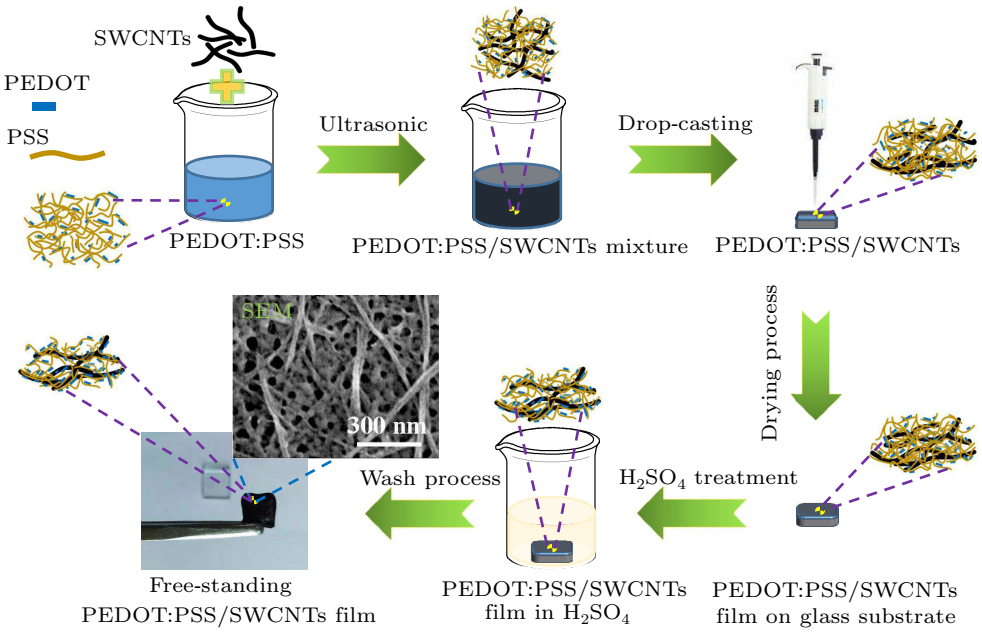


Fig. 1. Schematic illustration of the fabrication process of the porous PEDOT:PSS/SWCNTs film with high flexibility.

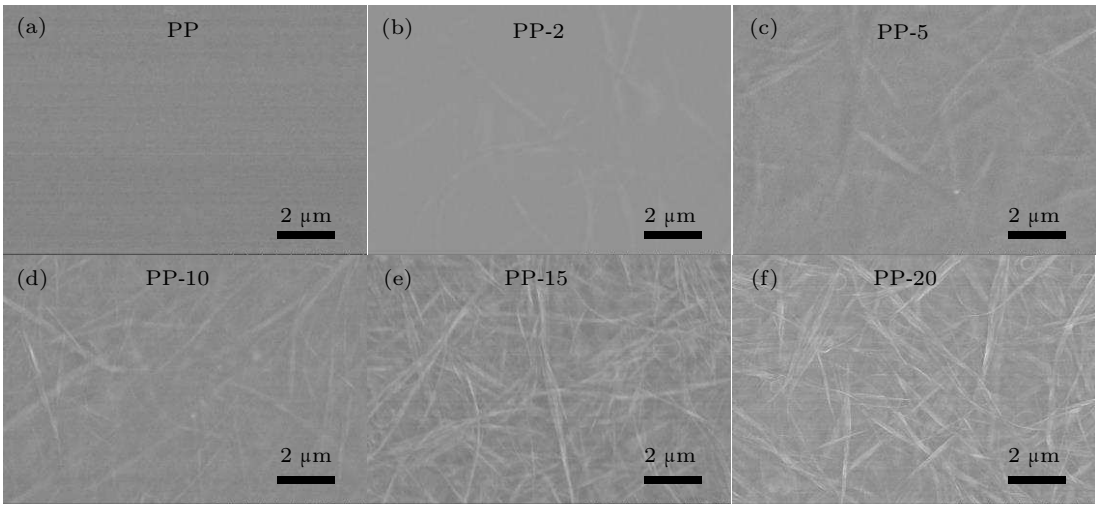


Fig. 2. SEM images of as-prepared PEDOT:PSS/SWCNTs films with different SWCNTs contents: (a) 0 wt% SWCNTs; (b) 2 wt% SWCNTs; (c) 5 wt% SWCNTs; (d) 10 wt% SWCNTs; (e) 15 wt% SWCNTs; (f) 20 wt% SWCNTs.

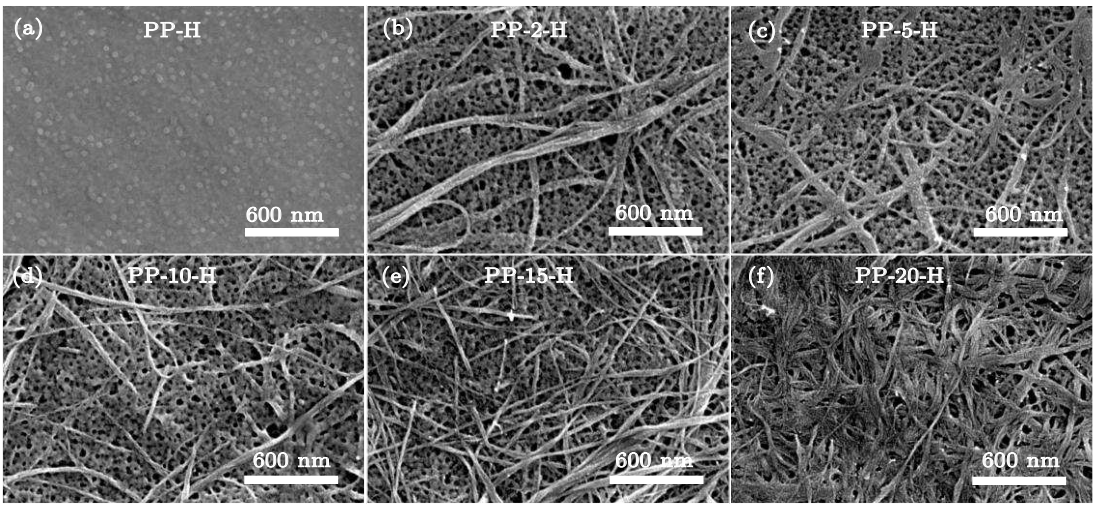


Fig. 3. SEM images of PEDOT:PSS/SWCNTs films with different SWCNTs contents after 24 h of H_2SO_4 treatment: (a) 0 wt% SWCNTs; (b) 2 wt% SWCNTs; (c) 5 wt% SWCNTs; (d) 10 wt% SWCNTs; (e) 15 wt% SWCNTs; (f) 20 wt% SWCNTs.

Namely, the conductive networks is not dense enough. With the CNTs loading increased to 10 wt%, they were found to uniformly distribute in the whole film, generating highly conductive continuous network with sufficient PEDOT:PSS/CNTs interfaces. By further increasing the SWCNTs content, some of them begin to aggregate both on the surface and inside the film.

After H_2SO_4 post-treatment, the surface topographies of PEDOT:PSS and the composite samples are very different. As shown in Fig. 3, SEM images of PEDOT:PSS thin films present some nanorods-like structures, which agrees well with that reported in the literature.[40] The formation of observed nanofibrils in PEDOT:PSS may be associated with the removal of PSS and the structural rearrangement during the concentrated H_2SO_4 soaking process.[40] It is noteworthy to point out that after the H_2SO_4 post-treatment, some submicron and nano-scale pores appear in the composite samples. Apparently, the appearance of the observed porous structure is directly related to the introduction of the SWCNTs, the hollow nanostructure of which may promote the penetration of the acid liquid in the composite samples. During the acid treatment, nanostructure of the conductive PEDOT:PSS was rearranged with removal of partial nonconductive PSS. Besides, some SWCNTs were partially embedded in the PEDOT:PSS component. With the help of SWCNTs, the above-mentioned processing of structural rearrangement in PEDOT:PSS could be effectively promoted. So that the variation and evolution of PEDOT:PSS morphologies would occur not only on the film surface but also in the internal part of the whole thin sample. In other words, the enhanced structural reorganization in PEDOT:PSS leads to the generation of the porous structures among the whole hybrid film.

To deeply understand such a change on the molecular level, the samples were characterized by using a nondestructive Raman spectroscopy, which is a powerful tool for studying conductive polymers and their composites. The Ra-

man spectra of pristine PEDOT:PSS and the as-prepared PEDOT:PSS/SWCNTs composites are presented in Fig. S1. For pristine PEDOT:PSS samples, 1432 cm^{-1} and 1499 cm^{-1} bands are characteristic of symmetric $C_\alpha{=}C_\beta(-O)$ stretching in the five-membered ring and asymmetric $C_\alpha{=}C_\beta$ stretching, respectively.[41] With incorporation of SWCNTs, the most significant difference is that the both peaks were blue-shifted. For example, in the composite containing 10 wt% of SWCNTs, the corresponding bands of PEDOT molecules shift distinctly to 1439 cm^{-1} and 1503 cm^{-1}, respectively. On the other hand, for the composite films, a sharp band centered at 1592 cm^{-1} with a shoulder broad band at 1576 cm^{-1} can be attributed to the G^+ and G^- bands, namely, longitudinal mode and circumferential mode of the semiconducting SWCNTs, respectively.[42] Notably, the raise of intensities for the two characteristic bands can be clearly observed with increasing the SWCNTs content of the composites. These band-shifts and the changes in band intensity show that the interfacial π–π interactions between PEDOT molecules and SWCNTs are relatively strong, which would facilitate the PEDOT:PSS molecules to be attached to the surface of SWCNTs.[42,43]

After the treatment by using sulfuric acid, the symmetric $C_\alpha{=}C_\beta$ stretching band in the composite samples was red-shifted, as shown in Fig. S2, which was quite similar to the situation that occurred during oxidation processes of PEDOT:PSS as well as doping treatment via dielectric solvents.[15,16,31,44,45] Generally, the shift of symmetric $C_\alpha{=}C_\beta$ stretching vibration (in the range of from 1432 cm^{-1} to around 1443 cm^{-1} in this work) is mainly associated with the relative proportion of benzoid and quinoid conformations, resulted from variation of the oxidation level of molecular structure and the degree of thiophene backbone deformation.[31,45] Because there is lack of conjugated π-electrons on $C_\alpha{-}C_\beta$, the band red-shift of symmetric $C_\alpha{=}C_\beta$ stretching implies that more quinoid structures exist in the composites as compared with the untreated samples.[44,46] It is well known that in an expanded/linear quinoid-dominated structure, it is easier for conjugated π-electrons to be delocalized over the whole PEDOT chain, in which the neighboring thiophene rings are oriented almost in the same plane, and thus providing improved charge-carrier mobility, rather than in a coil benzoid-dominated type.[16,31] Besides, after the acid treatment, significant rise in the corresponding band intensities can also be observed, which may be attributed to the oxidation or reorientation effect of sulfuric acid on PEDOT chains.[41,45,46] Moreover, as shown in Fig. S3, the band assigned to asymmetric $C_\alpha{=}C_\beta$ stretching in the treated samples, was gradually blue shifted with increasing the CNTs content, which can be interpreted by the strong interaction between the two components. Meanwhile, the band intensity significantly increases with increasing the SWCNTs content, and reaches a maximum value in the sample containing about 10 wt% SWCNTs, as shown in Fig. 4(a) and Fig. S3, illustrating that the incorporation of an appropriate amount of SWCNTs can reinforce the moderate oxidation processing and/or the reorientation effect of PEDOT molecular chains via a post-treatment of sulfuric acid. More detailed information about the variation of PEDOT:PSS/SWCNTs composites during the treatment processing will be discussed in the following sections.

UV-Vis spectra were applied to characterize the structure changes in PEDOT:PSS and PEDOT:PSS/SWCNTs hybrid films. As shown in Fig. S4, for the pristine PEDOT:PSS, absorbance peaks at 223 nm and 253 nm can be ascribed to the aromatic ring of –PSS group.[47] After treated by using H_2SO_4, both of the peaks are however not visible, which results from the removal of the nonconductive –PSS part. Figure 4(b) shows UV-Vis spectra of SWCNTS and PEDOT:PSS/SWCNTs hybrid films after 24 h of H_2SO_4 treatment. As the incorporation of SWCNTs, both of the peaks shift to higher wavelength direction, for instance, the peak at 253 nm shifts to 273 nm due to the strong π–π interactions between SWCNTs and PEDOT:PSS. Meanwhile, the peak intensity increases with the increasing of the SWCNTs content. According to Kang and the co-authors, the increase in UV region absorbance suggests that the optical transition occurs, which may be resulted from the addition of SWCNTs with highly mobile holes.[47,48]

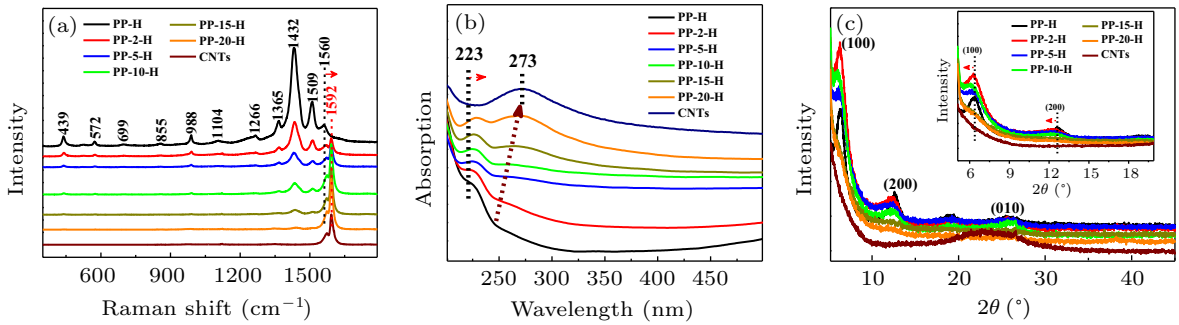


Fig. 4. (a) Raman spectra, (b) UV-Vis spectra, and (c) XRD patterns of SWCNTS and PEDOT:PSS/SWCNTs hybrid films after 24 h of H_2SO_4 treatment.

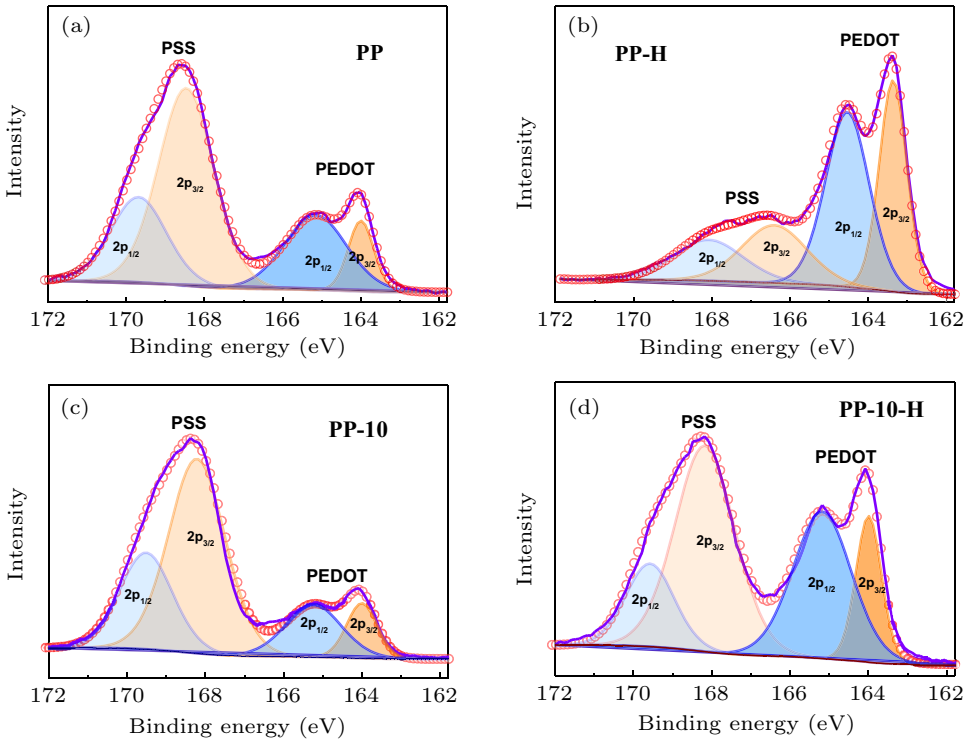


Fig. 5. The S 2p high resolution XPS spectra including fits for PEDOT and PSS: (a) pristine PEDOT:PSS, (b) sulfuric acid treated PEDOT:PSS, (c) the as-prepared PEDOT:PSS/SWCNTs hybrid sample containing 10 wt% SWCNTs, and (d) sample (c) treated by using H_2SO_4.

To further understand the effect of the SWCNTs incorporation on the structures of conductive PEDOT:PSS molecular, XRD patterns were examined to investigate the variation of their crystallization properties. For the pristine PEDOT:PSS (shown in Fig. S5), the XRD patterns only possess two faint characteristic peaks at 17.5° and 25.4°, associated with the amorphous halo of PSS and the interchain planar ring-stacking of PEDOT, respectively.[40,49] With incorporation of the SWCNTs, the intensity of the two peaks increases, which may be resulted from the strong interactions between the two components. After the post-treatment (see Fig. 4(c)), two novel characteristic peaks appear in the XRD patterns, that is, $2\theta = 6.3°$ and 12.6°, indexed to the lamella stacking (100) of two distinct alternate orderings components and its corresponding second-order peak (200), respectively.[40,49] After addition of the SWCNTs, the peaks at $2\theta = 6.3°$ and 12.6° shift to a lower angle with increased intensity (as shown in the inset of Fig. 4(c)), which indicates the increasing lamella stacking and improved crystallinity. The highly ordered pattern with strong reflective intensities would facilitate the transport of the hole charge in the continuous porous framework, and thus the increase of the electric conductivity. These changes can be ascribed to the removal effect of the sulfuric acid and the following molecular rearrangement.

XPS analysis was conducted to further elucidate the chemical composition changes during sulfuric acid treatment (shown in Fig. 5). For the high resolution S 2p spectra, there are two remarkable characteristic bands centered at binding energies of $\sim$ 169 eV and $\sim$ 164 eV, which are readily ascribed to the presence of PSS and PEDOT, respectively. It is worth noting that, the relative content of PSS to PEDOT on the film surface was obviously decreased. According to the previous reports, this ratio decrease is reflective of conformational variation of PEDOT:PSS arose from PSS removal in the processing of sulfuric acid treatment.[25,26,40,50] To quantify the effect of the PSS extraction, the ratios of PSS to PEDOT were estimated by calculating the integral area ration of the corresponding peaks. The highest PSS/PEDOT surface component ratios of 2.47 and 3.48 were obtained for the pristine PEDOT:PSS and PEDOT:PSS/SWCNTs (PP-10) films, whereas the post treatment using H_2SO_4 reduced the PSS/PEDOT ratio to 0.49 and 1.36 for the treated PEDOT:PSS and PEDOT:PSS/SWCNTs (PP-10-H) films, respectively. As is well known, the PSS part is non-conductive in nature, and thus plays a negative role on the electrical conductivity of PEDOT:PSS. Therefore, the decrease in the PSS content can tremendously increase the carrier concentration. Additionally, the decreased PSS component also leads to the structural rearrangement in PEDOT chains, resulting in more linear conformation and thus better crystallinity of the conductive polymers. All these changes can effectively improve the interchain and interdomain charge hopping between PEDOT grains, which will enhance the electron transport of PEDOT:PSS and the related composite films.[33,51]

Figure 6(a) shows the electrical conductivity (σ) of the as-prepared PEDOT:PSS/SWCNTs films as a function of SWCNTs. As can be seen, the pristine PEDOT:PSS film only presents a relative low electrical conductivity of around 0.14 $S \cdot cm^{-1}$, due to the disordered arrangement of the molecules (see Fig. S5). With incorporation of the SWCNTs,

the electrical conductivity of the composite films significantly increases. In this study, due to the acid pretreatment, SWCNTs can disperse well in PEDOT:PSS aqueous solution, and easily form more PEDOT:PSS/SWCNTs interfaces during the drying progress. Besides, the SWCNTs possess much higher electrical conductivity than the pristine PEDOT:PSS film. With increasing SWCNTs content, more efficient electrical pathways are fabricated resulted from the increase of the CNTs bundle connections (see Fig. 2).[35] When the weight ratio of SWCNTs is up to 20 wt% in this work, the electrical conductivity of the composite sample achieves a high value of 27.84 S·cm^{-1}, and continually increases with further increasing SWCNTs content in the composites (Fig. S6). Seebeck coefficient is an intrinsic factor determining the TE properties of the materials. As is presented in Fig. 6(b), the pristine PEDOT:PSS film reveals a Seebeck coefficient of 18.9 μV·K^{-1}, which is very similar to that of early reported PEDOT:PSS (19.4 μV·K^{-1}).[26] With addition of 2 wt% SWNCTs, the Seebeck coefficient decreased to around 16.1 μV·K^{-1}, and reduced slightly with continual increasing of the CNTs filler content. When the CNTs content was increased to 12.5 wt%, a minimum Seebeck coefficient of 14.9 μV·K^{-1} was obtained. This decline of the Seebeck coefficient can be ascribed to the dramatic increase of the carrier concentration with the SWCNTs incorporation. For example, the as-prepared PP-10 composite sample (containing 10 wt% SWCNTs) possesses a carrier concentration of 5.76×10^{19} cm^{-3} (shown in Fig. 7 and Table S1), which is much larger when compared with that of the pristine PEDOT:PSS (7.24×10^{18} cm^{-3}). Generally, the increase of carrier concentration may help to push Fermi level (E_F) into the conduction band, which in turn results in the decrease of the Seebeck coefficient.[26,52] Whereas, when further increasing the CNTs filler content, the Seebeck coefficient of the composite films appears to increase, for instance, composite samples PP-15 and PP-20 display 17.5 μV·K^{-1} and 16.8 μV·K^{-1}, respectively. The Seebeck coefficient only shows slight changes as increasing the CNTs loading content (Fig. 6 and Fig. S6), and thus the power factor is mainly associated with variation of the electrical conductivity. For samples with relatively low CNTs content ($\leq$ 20 wt%), a power factor of around 0.786 μW·m^{-1}·K^{-2} can be achieved (Fig. 6(c)). With the further rise in CNTs loading, the electrical conductivity of the composite films continuously increases since more efficient electrical pathways are created. As expected, the as-prepared composite films containing 90 wt% CNTs possess the highest power factor of 45.34 μW·m^{-1}·K^{-2} (Fig. S6(c)). Apparently, these values are not good enough to meet the high requirements of thermoelectric energy conversion.

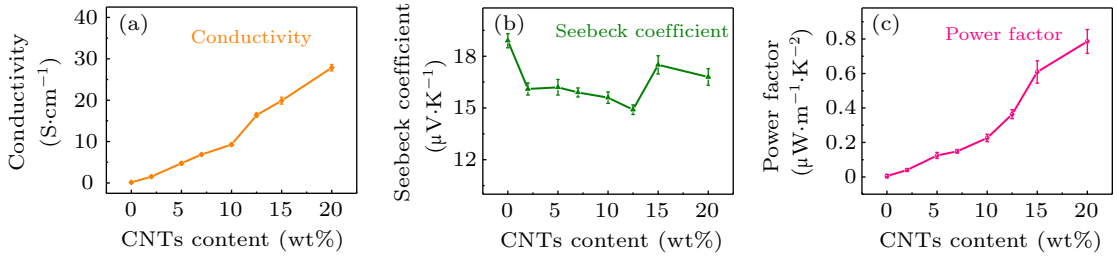


Fig. 6. TE performances of the PEDOT:PSS/SWCNTs films as a function of CNTs fractions before the post-treatment by using sulfuric acid.

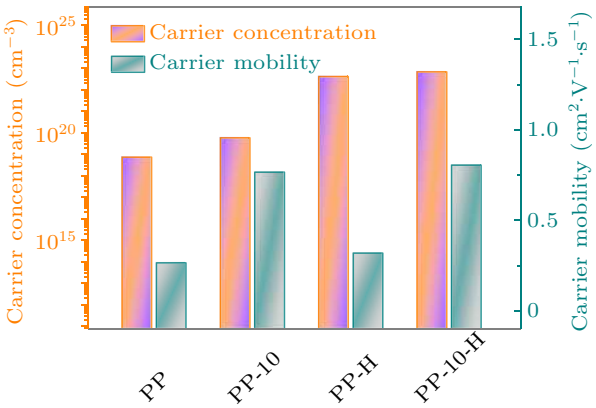


Fig. 7. Carrier concentration (n) and carrier mobility (μ) of PEDOT:PSS and the composite film containing 10 wt% SWCNTs before and after H_2SO_4 post-treatment, respectively.

In this study, a post-treatment using sulfuric acid is conducted to remove the PSS component, which is not conductive. As discussed above, the removal of PSS using H_2SO_4 also results in the structural rearrangement of the composite samples, and thus leads to improving of the crystallinity (Fig. 4(c)). All these structure characteristics are beneficial to the improvement of electrical conductivity. For example, the H_2SO_4 treated PEDOT:PSS films present an electrical conductivity of 1637.39 S·cm^{-1} in this work (Fig. 8(a)), which is 4 orders of magnitude higher than that of the pristine polymer film (around 0.14 S·cm^{-1}). Figure 8(a) also displays the variation of the electrical conductivity for composite samples as a function of CNTs content. It is clear that the conductivities of all composite films are dramatically improved through the post-treatment. Notably, the conductivity can also be greatly enhanced with the introduction of the SWCNTs, which is associated with the strong interfacial π–π interactions between the two components (Figs. 4(a) and 4(b)). With a gradual increase of the CNTs filler ratio, integrated conductive continuous network is steadily fabricated, due to the formation of more effective PEDOT:PSS/CNTs interfaces. As a result, the electrical conductivity continually increases and achieves a maximum value of 4333.33 S·cm^{-1} when the fraction of SWCNTs is increased to 10 wt%. How-

ever, with further increase of the content of SWCNTs in the PEDOT:PSS/SWCNTs composites, for example, when the CNTs content is up to 15 wt% and 20 wt%, visible agglomeration of carbon nanotubes appears. In particular, in samples containing 20 wt% CNTs, almost the whole field of view is covered with carbon nanotubes (Fig. 3), which is not conductive to the formation of high-efficient organic/inorganic interface and thus leads to obvious decrease of the σ value. As expected, PP-15-H and PP-20-H samples only show electrical conductivity of 1875.02 S·cm^{-1} and 1865.03 S·cm^{-1}, respectively. It is of interest to note that the CNTs films prepared in this work only present a relatively low σ value of around 1714.28 S·cm^{-1}, which is much smaller than that of single-walled CNTs (e.g., 10^4-10^5 S·cm^{-1}).[34,53] This may be associated with the low packing density of SWCNTs in the SWCNTs film. In another word, a contact resistance at junctions of SWCNTs or their bundles is the main reason leading to the low conductivity of the CNTs. For composite films, PEDOT:PSS molecular with ordered arrangement tightly adheres to CNTs surface and forms continuous conductive networks with more sufficient and better-connected pathways. Though porous structure may partly reduce the number of conducting channels, more efficient networks for charge transport have been successfully fabricated via sulfuric acid post-treatment.

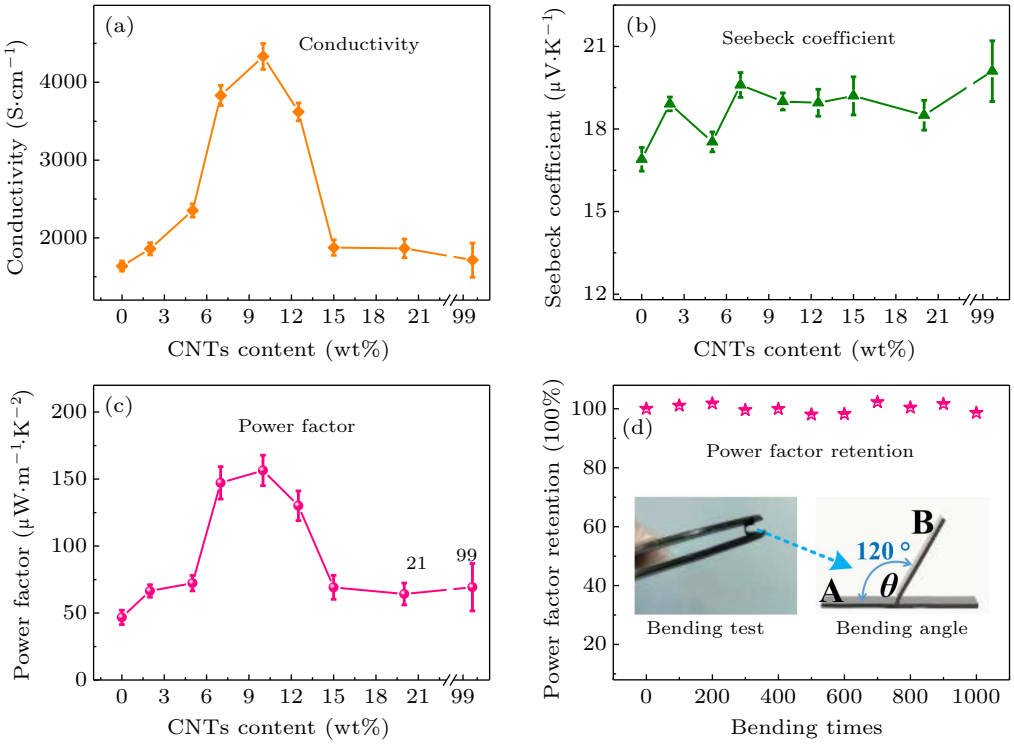


Fig. 8. TE properties of H_2SO_4 treated PEDOT:PSS/SWCNTs hybrid films as a function of CNTs fractions.

For H_2SO_4 treated PEDOT:PSS/SWCNTs films, the Seebeck coefficient changes in a narrow range of 17.5–19.6 μV·K^{-1} (as shown in Fig. 8(b)), without obvious variation trends as a function of SWCNTs fraction. This may be associated with the morphologies of the nanocomposite films and the charge transport features between the CNTs and the ordered structure of PEDOT:PSS. Notably, these values are around 3 μV·K^{-1}, higher than those of untreated samples ranging from 14.9 μV·K^{-1} to 16.8 μV·K^{-1}. Notably, the post-treatment using sulfuric acid can dramatically enhance the carrier concentration and the carrier mobility of the PEDOT:PSS/SWCNTs composites (see Fig. 7 and Table S1) simultaneously, due to the removal of the non-conductive PSS part and an accompanying molecular rearrangement of PEDOT:PSS. As reported, an ordered molecular structure with high carrier mobility is vital for realizing excellent TE performance in conducting polymers and their composites. Whereas, the significant removal of non-conductive PSS also leads to the increase of carrier concentration (Fig. 7 and Table S1). In general, an increase in carrier concentration would push the Fermi level (E_F) to the conduction band, which in turn results in a reduced Seebeck coefficient.[26,52] On the other hand, effective potential barriers at PEDOT:PSS/SWCNTs interfaces may increase possibility for the energy-dependent scattering of electrical carriers, namely, an energy filtering effect. Besides, crystallite boundaries around the SWCNTs also preferentially allow the carriers with high energy to pass, and thereby resulting in the increase of the mean carrier energy and the Seebeck coefficient.[12,54] These two competitive mechanisms may affect the Seebeck coefficient at the same time. Apparently, it is the energy filtering effect that plays the crucial role in the enhancement of the Seebeck coefficient, rather than the variation of E_F induced via carrier concentration increasing. Due to the slight

changes in Seebeck coefficient, the power factor is mainly associated with the electrical conductivity. As a consequence, a maximum power factor of 156.43 $\mu W \cdot m^{-1} \cdot K^{-2}$ is achieved for the sample containing 10 wt% CNTs at room temperature (Fig. 8(c)), which is around 2 orders of magnitude higher than that of the untreated sample. This outstanding TE performance is comparable with or even better than other PEDOT:PSS/CNT composites films (as shown in Table 1).[30,31,33–37,55]

Table 1. TE properties of PEDOT:PSS/CNTs films.

Component	Preparing method	σ ($S \cdot cm^{-1}$)	S ($\mu V \cdot K^{-1}$)	PF ($\mu W \cdot m^{-1} \cdot K^{-2}$)	Ref.
PEDOT:PSS/SWCNT	DMSO doping and direct mixing	400	~ 25	~ 25	[30]
PEDOT:PSS/SWCNTs	DMSO doping and Layer by layer casting	241	38.9	21.1	[31]
EG treated CNT/PEDOT:PSS	Direct mixing, drop casting and EG treatment	~ 780	~ 43.7	~ 151	[35]
DMSO treated SWCNT/PEDOT:PSS	Dilution filtration and DMSO treatment	745.4	~ 33.4	108.7	[36]
DMSO treated PEDOT:PSS/SWCNT	Direct mixing and DMSO treatment	3800	28	300	[34]
SWNTs/DMSO-PEDOT:PSS	DMSO doping and vacuum filtration	~ 535	44.3	105	[33]
PEDOT:PSS/SWCNT	Vacuum filtration and H_2SO_4 treatment	510.6	20.18	20.68	[37]
PEDOT:PSS/SWCNTs	Ethanol addition and dilution filtration	~ 900	~ 30.5	83.9	[55]
H_2SO_4 treated PEDOT:PSS/SWCNT	Drop casting and H_2SO_4 treatment	4333.33	~ 19.2	~ 156.43	this work

Thermal conductivity is another important parameter that governs the thermoelectric conversion efficiency of TE materials. As reported, the carbon nanotubes generally possess a high intrinsic thermal conductivity of around 10^3 $W \cdot m^{-1} \cdot K^{-1}$, which makes them irrelevant for direct TE applications.[56] Fortunately, when combined with polymers, the obtained composites often show ultra-low thermal conductivity. For example, CNT/PANI nanocomposites possess a thermal conductivity of 0.45 $W \cdot m^{-1} \cdot K^{-1}$,[57] PVAc/MWCNT composites with stabilizer deliver a thermal conductivity of ~ 0.17–0.22 $W \cdot m^{-1} \cdot K^{-1}$,[58] while PEDOT:PSS/SWCNTs composites have a thermal conductivity of 0.2–0.7 $W \cdot m^{-1} \cdot K^{-1}$.[59–62] All these results are very close to values of polymer component (~ 0.4 $W \cdot m^{-1} \cdot K^{-1}$) rather than those of CNTs part, namely, the thermal conductivity for composites is relatively insensitive to the CNTs type and concentration.[31,63] In our present work, the relatively low SWCNTs loadings suggest that many of tube–tube junctions are connected by PEDOT:PSS matrix, making less favorable paths for thermal energy transport.[60,61] In addition, polymers like PEDOT:PSS possess different vibrational frequencies from those of SWCNTs, which impedes phonon transport across SWCNT-PEDOT:PSS-SWCNT interfaces.[60–62] Meanwhile, phonon can also be scattered at the polymer/SWCNT interface, resulting in a low thermal conductivity.[59,64] Moreover, a large number of pores are observed in submicron- and nano-scale (see Fig. 3). Theoretically, such a porous structure is crucial to produce phonon scattering and reduce thermal conductivity, without obviously sacrificing electrical properties.[37] Therefore, the thermal conductivity of porous PEDOT:PSS/SWCNTs films is expected to be kept at a relatively low level. Notably, after bending for 1000 times at a bending angle of around 120° (the bending angel θ is defined as the angle between plane A and plane B, shown in the inset of Fig. 8(d)), the retention of the power factor still remains at ~ 98.5% (Fig. 8(d) and Fig. S7), revealing good flexibility of the treated film. This may be correlated with the strong π–π interactions between the two components and the porous structure of the treated samples.

4. Conclusion and perspectives

In summary, highly flexible, free-standing, porous PEDOT:PSS/SWCNTs composite films were successfully fabricated through solution drop-casting method and a subsequent sulfuric acid treatment. Due to the attachment of conducting polymer molecular tightly to the CNTs surface, more sufficient conductive networks were successfully fabricated and thus the hybrid porous films possessed high electrical conductivities. In addition, the Seebeck coefficient of the composite structures varied in a narrow range of 17.5–19.6 $\mu V \cdot K^{-1}$. As a result, the power factor generally exhibited a similar variation tendency to that of the electrical conductivity, and achieved a high value of 156.43 $\mu W \cdot m^{-1} K^{-2}$ via adjusting the CNTs content. Besides, due to the porous structure and the strong π–π interactions between the two components, the composite film possessed good flexibility. This work provides an effective strategy to significantly increase the thermoelectric efficiency of composite materials via construction of efficient conductive networks with porous nanostructure, benefiting the developments and applications of TE materials.

Acknowledgment

Project supported by the National Natural Science Foundation of China (Grant Nos. U2004174, 51773118, and 51673044).

References

[1] Zhang Q, Sun Y, Xu W and Zhu D 2014 *Adv. Mater.* **26** 6829
[2] Tang J, Chen R, Chen L, Bazan G C and Liang Z 2020 *J. Mater. Chem. A* **8** 9797
[3] Zhang Y, Chen S, Zhang H, Ding X, Fu P and Du F 2021 *Compos. Commun.* **27** 100883
[4] Li C, He W, Wang D and Zhao L D 2021 *Chin. Phys. B* **30** 067101
[5] Xia X G, Zhang Q, Zhou W B, Xiao Z J, Xi W, Wang Y C and Zhou W Y 2021 *Chin. Phys. B* **30** 078801

[6] Gao C and Chen G 2016 *Compos. Sci. Technol.* **124** 52
[7] Wang L, Pan C, Chen Z, Zhou W, Gao C and Wang L 2018 *ACS Appl. Energ. Mater.* **1** 5075
[8] Tang J, Chen Y, McCuskey S R, Chen L, Bazan G C and Liang Z 2019 *Adv. Electron. Mater.* **5** 1800943
[9] Li Y, Du Y, Dou Y, Cai K and Xu J 2017 *Synthetic Met.* **226** 119
[10] Wang L, Yao Q, Xiao J, Zeng K, Qu S, Shi W, Wang Q and Chen L 2016 *Chem. Asian. J* **11** 1804
[11] Wang H, Yi S i and Yu C 2016 *Polymer* **97** 487
[12] Zhou X, Pan C, Liang A, Wang L and Wong W Y 2017 *Compos. Sci. Technol.* **145** 40
[13] Kishi N, Kondo Y, Kunieda H, Hibi S and Sawada Y 2017 *J. Mater. Sci. Mater. Electron.* **29** 4030
[14] Zhu Z, Liu C, Jiang F, Xu J and Liu E 2017 *Synthetic Met.* **225** 31
[15] Ouyang J, Xu Q, Chu C W, Yang Y, Li G and Shinar J 2004 *Polymer* **45** 8443
[16] Ouyang J, Chu C W, Chen F C, Xu Q and Yang Y 2005 *Adv. Funct. Mater.* **15** 203
[17] Badre C, Marquant L, Alsayed A M and Hough L A 2012 *Adv. Funct. Mater.* **22** 2723
[18] Liu C, Xu J, Lu B, Yue R and Kong F 2012 *J. Electron. Mater.* **41** 639
[19] Xia Y and Ouyang J 2009 *Macromolecules* **42** 4141
[20] Fan Z, Du D, Yu Z, Li P, Xia Y and Ouyang J 2016 *ACS Appl. Mater. Interfaces* **8** 23204
[21] Lee S H, Park H, Kim S, Son W, Cheong I W and Kim J H 2014 *J. Mater. Chem. A* **2** 7288
[22] Kim G H, Shao L, Zhang K and Pipe K P 2013 *Nat. Mater.* **12** 719
[23] Crispin X, Jakobsson F L E, Crispin A, Grim P C M, Andersson P, Volodin A, Van Haesendonck C, Van der Auweraer M, Salaneck W R and Berggren M 2006 *Chem. Mater.* **18** 4354
[24] Takano T, Masunaga H, Fujiwara A, Okuzaki H and Sasaki T 2012 *Macromolecules* **45** 3859
[25] Bießmann L, Saxena N, Hohn N, Hossain M A, Veinot J G C and Müller-Buschbaum P 2019 *Adv. Electron. Mater.* **5** 1800654
[26] Bae E J, Kang Y H, Jang K S and Cho S Y 2016 *Sci. Rep.* **6** 18805
[27] Liu X, Du Y, Meng Q, Dou Y, Jin M, Xu J and Shen S Z 2020 *Adv. Eng. Mater.* **22** 2000605
[28] Zhang Y, Liu S, Koh J J and He C 2021 *J. Materiomics* **7** 34
[29] Zhang Y, Zhang Q and Chen G 2020 *Carbon Energy* **2** 408
[30] Kim D, Kim Y, Choi K, Grunlan J C and Yu C 2010 *ACS Nano* **4** 513
[31] Song H, Liu C, Xu J, Jiang Q and Shi H 2013 *RSC Adv.* **3** 22065
[32] Zhang Z, Chen G, Wang H and Li X 2015 *Chem. Asian. J.* **10** 149
[33] Jiang Q, Lan X, Liu C, Shi H, Zhu Z, Zhao F, Xu J and Jiang F 2018 *Mater. Chem. Front.* **2** 679
[34] Zhang L, Harima Y and Imae I 2017 *Org. Electron.* **51** 304
[35] Lee W, Kang Y H, Lee J Y, Jang K S and Cho S Y 2016 *RSC Adv.* **6** 53339
[36] Du Y, Shi Y, Meng Q and Shen S Z 2020 *Synthetic Met.* **261** 116318
[37] Wei S, Huang X, Deng L, Yan Z C and Chen G 2021 *Compos. Sci. Technol.* **208** 108759
[38] Jia F, Wu R, Liu C, Lan J, Lin Y H and Yang X 2019 *ACS Sustainable Chem. Eng.* **7** 12591
[39] Sun X, Wei Y, Li J, Zhao J, Zhao L and Li Q 2017 *Sci. China Mater.* **60** 159
[40] Kim N, Kee S, Lee S H, Lee B H, Kahng Y H, Jo Y R, Kim B J and Lee K 2014 *Adv. Mater.* **26** 2268
[41] Farah A A, Rutledge S A, Schaarschmidt A, Lai R, Freedman J P and Helmy A S 2012 *J. Appl. Phys.* **112** 113709
[42] Fan W, Guo C Y and Chen G 2018 *J. Mater. Chem. A* **6** 12275
[43] Yoo D, Kim J, Lee S H, Cho W, Choi H H, Kim F S and Kim J H 2015 *J. Mater. Chem. A* **3** 6526
[44] Łapkowski and Proń A 2000 *Synthetic Met.* **110** 79
[45] Garreau S, Louarn G, Buisson J P, Froyer G and Lefrant S 1999 *Macromolecules* **32** 6807
[46] Ely F, Matsumoto A, Zoetebier B, Peressinotto V S, Hirata M K, de Sousa D A and Maciel R 2014 *Org. Electron.* **15** 1062
[47] Mahakul P C, Sa K, Das B, Subramaniam B V R S, Saha S, Moharana B, Raiguru J, Dash S, Mukherjee J and Mahanandia P 2017 *J. Mater. Sci.* **52** 5696
[48] Kang K S, Lim H K, Cho K Y, Han K J and Kim J 2008 *J. Phys. D: Appl. Phys.* **41** 012003
[49] Kim N, Lee B H, Choi D, Kim G, Kim H, Kim J R, Lee J, Kahng Y H and Lee K 2012 *Phys. Rev. Lett.* **109** 106405
[50] Wang J, Cai K and Shen S 2014 *Org. Electron.* **15** 3087
[51] Suchand Sangeeth C S, Jaiswal M and Menon R 2009 *J. Phys. Condens. Matter* **21** 072101
[52] Bubnova O and Crispin X 2012 *Energ. Environ. Sci.* **5** 9345
[53] Yang J, Yip H L and Jen A K Y 2013 *Adv. Energ. Mater.* **3** 549
[54] See K C, Feser J P, Chen C E, Majumdar A, Urban J J and Segalman R A 2010 *Nano Lett.* **10** 4664
[55] Song H, Qiu Y, Wang Y, Cai K, Li D, Deng Y and He J 2017 *Compos. Sci. Technol.* **153** 71
[56] Kim P, Shi L, Majumdar A and McEuen P L 2001 *Phys. Rev. Lett.* **87** 215502
[57] Meng C, Liu C and Fan S 2010 *Adv. Mater.* **22** 535
[58] Moriarty G P, Wheeler J N, Yu C and Grunlan J C 2012 *Carbon* **50** 885
[59] Wang J, Cai K, Yin J and Shen S 2017 *Synthetic Met.* **224** 27
[60] Yu C, Choi K, Yin L and Grunlan J C 2011 *ACS Nano* **5** 7885
[61] Kim D, Kim Y, Choi K, Grunlan J C and Yu C 2010 *ACS Nano* **4** 513
[62] Moriarty G P, De S, King P J, Khan U, Via M, King J A, Coleman J N and Grunlan J C 2013 *J. Polym. Sci. Pol. Phys.* **51** 119
[63] Jiang F X, Xu J K, Lu B Y, Xie Y, Huang R J and Li L F 2008 *Chin. Phys. Lett.* **25** 2202
[64] Bounioux C, Díaz-Chao P, Campoy-Quiles M, Martín-González M S, Goñi A R, Yerushalmi-Rozen R and Müller C 2013 *Energy Environ. Sci.* **6** 918